Science of the Total Environment 962 (2025) 178440

Contents lists available at ScienceDirect

Science of the Total Environment

journal homepage: www.elsevier.com/locate/scitotenv

Enhanced mercury deposition in Arctic Alaskan lake sediments coincides with early Holocene hydroclimate shift

Melissa Griffore [a,*], Mark Abbott [a], Eitan Shelef [a], Matthew Finkenbinder [b], Joseph Stoner [c], Mary Edwards [d]

[a] Department of Geology and Environmental Science, University of Pittsburgh, Pittsburgh, PA, USA
[b] Department of Biology and Earth Systems Science, Wilkes University, Wilkes Barre, PA, USA
[c] College of Earth, Ocean, and Atmospheric Sciences, Oregon State University, Corvallis, OR, USA
[d] School of Geography and Environmental Science, University of Southampton, UK

HIGHLIGHTS

- Early Holocene Hg mobilization linked to increased precipitation and permafrost thaw.
- Evidence of dissolved Fe, Mn, and Hg associated with saturated active layer.
- Catchment vegetation change influences lake sediment Hg concentrations.
- Modern sixfold Hg flux increase attributed to anthropogenic Hg and climate factors.

GRAPHICAL ABSTRACT

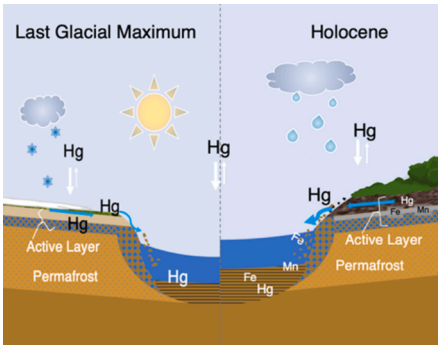

ARTICLE INFO

Editor: Philiswa Nomngongo

Keywords:
Paleoenvironmental Hg archive
Permafrost thaw
Arctic watershed mercury dynamics
Anthropogenic climate warming
Waterlogged active layer
Redox-sensitive metals

ABSTRACT

Substantial amounts of mercury (Hg) are projected to be released into Arctic watersheds as permafrost thaws amid warmer and wetter conditions. This may have far-reaching consequences because the highly toxic methylated form of Hg biomagnifies rapidly in ecosystems. However, understanding how climate change affects Hg dynamics in permafrost regions is limited due to the lack of long-term Arctic Hg records. Using a 27-ka Hg sediment record from Burial Lake, northwestern Alaska, we examine how well-characterized temperature, precipitation, and vegetation shifts affected Hg mobilization in a catchment underlain by permafrost. During the Last Glacial Maximum (29.6–19.6 ka), Hg concentrations (63 ± 5 μg/kg) and Hg flux (8.6 ± 2.2 μg m^{-2} yr^{-1}) remain relatively stable. Abrupt warming trends, starting at 17.6 ka, do not coincide with Hg levels. After 15 ka, the ecosystem transitions to shrub tundra, Hg concentrations (101.2 μg/kg) peak at 14.2 ka, while flux (5.3 ± 1.3 μg m^{-2} yr^{-1}) declines and stabilizes. At ~11 ka, increased precipitation coincides with a 72 % rise in Hg concentrations and a 32 % increase in Hg flux compared to average Hg levels since 15 ka. These results suggest that summer rainfall was the primary driver of Hg mobilization from the catchment, while the vegetation shift influenced lake sediment Hg concentrations. At 1990 CE, peak Hg levels represent an 88 % increase in Hg concentrations (196.3 μg/kg) and a sixfold rise in Hg flux (38.1 μg m^{-2} yr^{-1}) above background levels,

* Corresponding author.
E-mail address: meg130@pitt.edu (M. Griffore).

https://doi.org/10.1016/j.scitotenv.2025.178440
Received 25 August 2024; Received in revised form 14 December 2024; Accepted 7 January 2025
Available online 14 January 2025

underscoring the need for further research to understand Hg dynamics driven by anthropogenic Hg emissions and climate change.

1. Introduction

Permafrost (perennially frozen) soils in the Arctic constitute one of Earth's largest surficial Hg reservoirs, containing over twice the amount of Hg sequestered in the ocean and lower latitude soils (Lim et al., 2020; Olson et al., 2018; Schaefer et al., 2020; Schuster et al., 2018). Mounting evidence of rapid permafrost degradation and increased precipitation in response to recent climate warming (Bintanja, 2018; Biskaborn et al., 2019; Gudmundsson et al., 2022; McCrystall et al., 2021) has led to concern over an elevated influx of Hg to Arctic surface waters (Schuster et al., 2011; Rydberg et al., 2010; Burke et al., 2018; St. Pierre et al., 2018, 2019; Staniszewska et al., 2022; Smith et al., 2024). Furthermore, it is thought that organic matter (OM) released from thawing permafrost could promote ideal conditions for producing methylmercury (MeHg) in terrestrial and aquatic ecosystems (Gordon et al., 2016; Jonsson et al., 2022). This Hg compound biomagnifies rapidly in food webs and is highly toxic to wildlife and humans.

A recent circumpolar Arctic study reported significant Hg exposure risks in freshwater fish, including Arctic char, lake trout, and northern pike (Barst et al., 2022). Among fish with the highest Hg concentrations, 36 % were classified as “high risk” and 5 % as “severe risk” for toxicity (Barst et al., 2022). These findings suggest that elevated Hg in Arctic surface waters could present substantial challenges for communities that depend on freshwater fish for sustenance. Despite these concerning findings, the impact of Arctic warming on the release of Hg from permafrost remains uncertain. The absence of long-term data documenting how climate change affects the Hg cycle in permafrost regions represents an important research gap, limiting our ability to assess ongoing changes and develop models to predict future scenarios.

Warming temperatures and the intensification of the hydrological cycle are expected to enhance Hg mobilization from thawing permafrost into Arctic lakes and rivers (Mu et al., 2020; Schuster et al., 2011; St. Pierre et al., 2018; Thompson et al., 2023). However, to date, the only published long-term Arctic lake sediment Hg records that span the Holocene are from Baffin Island, Nunavut, Canada (Cooke et al., 2012). A sediment record from Lake CF3, beginning at 11.5 ka, found that Hg concentrations increased at 9.5 ka following a twofold increase in OM and that Hg accumulation rates (Hg flux) remained low and stable throughout the preindustrial Holocene (Cooke et al., 2012). Additionally, a sediment record from the nearby Lake CF8, recorded heightened Hg and OM concentrations during the early Holocene, coinciding with increased catchment erosion and higher trace metal concentrations (Cooke et al., 2012; Wilson et al., 2012).

Long-term records from non-Arctic periglacial environments offer different insights. For example, a Hg record spanning 14.7 to 11.0 ka from Laguna de Los Anteojos, Venezuela, records a twofold rise in Hg concentrations and a fourfold increase in Hg flux around the end of the Younger Dryas (Schneider et al., 2020). The increased sediment Hg is attributed to an elevated atmospheric deposition rate, possibly related to increased air temperature, precipitation, or ocean ventilation activity (Schneider et al., 2020). Additionally, authors of a 17.3 ka-long Hg record from Lake Hambre, Chile, attribute heightened Hg flux and Hg concentrations to increased precipitation and leaching of Hg complexed with OM from catchment soils (Hermanns et al., 2013; Hermanns and Biester, 2013). While these studies provide important insights into the factors influencing Hg mobilization and deposition in watersheds affected by changing climate, the specific processes driving Hg dynamics in Arctic watersheds impacted by permafrost degradation remain poorly understood.

Northern Alaska is one of the few high-latitude regions that remained unglaciated during the last glacial cycle (Hamilton, 2010). The climate at Burial Lake throughout the Last Glacial Maximum (LGM; 29.6–19.6 ka) was more continental, colder, and dryer than today because the exposed Bering Land Bridge increased the distance from the coastline and precipitation sources (Gaglioti et al., 2017; Mann et al., 2001; Fig. 1B). In contrast, Burial Lake's proximity to the marginal seas today helps moderate the climate by supplying moisture and regulating temperatures (Fig. 1A). Hence, this study site is ideally situated to capture regional environmental changes driven by multi-century to millennial-scale transitions during post-glacial warming, including precession-driven increased solar insolation during the Boreal summer (Berger and Loutre, 1991; Laskar et al., 2004), rising sea levels (Jakobsson et al., 2017; Lambeck et al., 2014; Praetorius et al., 2020), and modulations in atmospheric and oceanic circulation patterns (Bartlein et al., 2015; Lora et al., 2016).

This study introduces a 27-ka sediment Hg record from Burial Lake, currently the only continuous Arctic Hg archive extending into the LGM. This lake sediment record has been thoroughly researched and is the focus of numerous published works (Abbott et al., 2010; Dorfman et al., 2015; Finkenbinder et al., 2018, 2015; King et al., 2022; Kurek et al., 2009; Shelef et al., 2022). Leveraging this extensive dataset, we investigate how abrupt changes in air temperature, vegetation, and precipitation are connected to the mobilization of Hg from the watershed, as evidenced by variations in lake sediment Hg concentrations and flux (Fig. 2C and D).

The Burial Lake sediment archive offers the first insights into factors that may have affected Hg mobilization in a permafrost-affected catchment during the late Pleistocene and early Holocene. Elevated Hg levels (Hg concentrations and Hg flux), in lake sediments or Arctic surface waters have been linked to factors attributed to warming air temperatures, including increased atmospheric deposition rates (Dastoor et al., 2022; Schneider et al., 2020), accelerated permafrost thaw (Mu et al., 2020; Schaefer et al., 2020; Schuster et al., 2018), and higher rates of erosion (Cooke et al., 2012; Smith et al., 2024; Wilson et al., 2012). The Burial Lake temperature reconstruction inferred from chironomids suggests that regional midsummer temperatures began to rise as early as 17.6 ka, and by 12.7 ka they had increased by 4.7 °C, surpassing present-day levels (Kurek et al., 2009; Fig. 2B). Therefore, we anticipated an increase in lake sediment Hg levels during this period.

The impact of vegetation types on Hg dynamics in Arctic soils remains poorly understood. However, in temperate regions, higher Hg loads in soils and watersheds have been attributed to more densely vegetated, productive ecosystems (Obrist et al., 2016; Olson et al., 2019; Zhou et al., 2021). The Burial Lake pollen record indicates a rapid vegetation transition from herbaceous tundra to shrub tundra beginning ~15.0 ka, coinciding with increased terrestrial OM composition in the lake sediments (Abbott et al., 2010; Finkenbinder et al., 2015; Fig. 3F). Hence, we expected this ecosystem shift to result in higher lake sediment Hg levels.

Research in subarctic Alaskan wetlands and boreal forest soils found that precipitation events enhanced the mobilization of Hg, likely bound to dissolved organic matter (DOM), from organic-rich soils (Åkerblom et al., 2008; Oswald and Branfireun, 2014; Poulin et al., 2019). A rapid decrease in chironomid-derived oxygen isotope ($\delta^{18}O_{chiro}$) values, combined with evidence for the onset of overflowing lake levels, is interpreted as indicating a region-wide hydroclimate shift at ~11.0 ka toward wetter conditions (Fig. 4F; Abbott et al., 2010; Finkenbinder et al., 2015; King et al., 2022). We hypothesize that increased precipitation would enhance the transport of dissolved materials from catchment soils to the lake, leading to elevated sediment Hg levels. The 27-ka Hg record from Burial Lake provides a unique opportunity to investigate the complex interactions among changes in climate, permafrost

dynamics, vegetation, and Hg mobilization in a watershed underlain by continuous permafrost. Examining these factors offers valuable insight into the potential impacts of ongoing Arctic warming on the contemporary Hg cycle.

2. Materials and methods

2.1. Study site

Burial Lake (68.43°N, 159.17°W; 460 m above sea level (ASL)) is a relatively small (0.8 km^2), hydrologically-open, oligotrophic lake located in the northwestern Brooks Range of Alaska (Fig. 1A). This region is underlain by continuous permafrost, with the active layer (the seasonally thawed layer above the permafrost) reaching a maximum depth of ~0.5 m (Pastick et al., 2015). The lake has a maximum depth of 21.5 m and a small catchment of 3.3 km^2 that slopes gently to the south. Poorly developed channels drain toward the lake from the north, and a small outlet stream flows to the southwest (see Supporting Information (SI) Fig. S1). The estimated mean annual air temperature (MAAT), based on 2014–2020 records from the Ivotuk meteorological station (581 m ASL; National Oceanic and Atmospheric Administration GHCND Network station USW00026564), located 136 km east of Burial Lake, ranges between −7 and − 9 °C, while the average difference between January and July temperatures is ~33 °C (King et al., 2022; Menne et al., 2012). Annual precipitation in this region totals 291 mm, with 63 % falling as rain between May and August (King et al., 2022; Menne et al., 2012). The lake remains frozen for nine months annually, with snow usually starting to accumulate by October (Finkenbinder et al., 2015). Detailed information about the Burial Lake setting, paleoclimate, and environmental reconstructions can be found in Kurek et al. (2009), Abbott et al. (2010), Dorfman et al. (2015), Finkenbinder et al. (2018, 2015), King et al. (2022), and Shelef et al. (2022).

2.2. Chronology

To establish a comprehensive chronological framework for the Burial Lake sediment record, we developed a composite age model by using recently measured and previously published radiocarbon dates from composite A-10/C-10 core (Finkenbinder et al., 2015) and integrated them with radiocarbon dates from the A-98, GL-98, and C-98 core (Abbott et al., 2010; SI Fig. S2; Table S1). Twenty-eight radiocarbon dates were used from bulk and macrofossil samples, including wood, seeds, and other plant material. Samples and standards were chemically pretreated, vacuum sealed, and combusted at the University of Pittsburgh according to standard protocols (Abbott and Stafford, 1996). The samples were then graphitized and dated by accelerator mass spectrometry at the W.M. Keck Carbon Cycle Accelerator Mass Spectrometry (AMS) facility at the University of California, Irvine. Surface samples from the A-10 core were dated using a broad–energy germanium detector (Canberra BE-3825) at the University of Pittsburgh. The ^{210}Pb and ^{214}Pb activities of 12 samples from the top 5.5 cm were measured (SI Table S2). Sediment ages were then determined using a constant rate of supply (CRS; Appleby and Oldfield, 1983). Bayesian age-depth modeling was performed using the BACON version 3.1.0 R software package employing the IntCal 20 calibration curve (Blaauw and Christen, 2011; Reimer et al., 2020).

2.3. Mercury analysis

Sediment samples from the Burial Lake composite core A-10/C-10 were taken at depth intervals ranging between 0.5 and 1 cm from the top 20 cm and between 1 and 5 cm for the remainder of the record, except where sediment was limited. The samples were then lyophilized and manually homogenized. Concentrations of total Hg were determined using a direct mercury analyzer (DMA-80) at the University of Pittsburgh, Department of Geology and Environmental Science. Blanks, duplicates, and standard reference materials (SRM; MESS-4, marine sediment) were run every tenth sample. The mean SRM value was 90.8 μg/kg, within 5 % of the reference value. The relative percent difference between duplicates ($n = 57$) was <5.5 %.

2.4. Data processing and statistical analysis

Given the varying age intervals for the sediment proxies from Burial Lake, we linearly interpolated the composite dataset to 140-year intervals in accordance with the median of 136.5-year Hg concentration sampling resolution. Using this time interval, the interpolated dataset comprises approximately 20 % of the data for the more highly resolved proxies, such as the XRF data. We used this interpolated dataset to construct correlation plots for the data spanning the entire 27-ka record and for the period from 17.0 to 9.0 ka using Pearson's correlation coefficient (r, $p < 0.05$; SI Fig. S3 and S4) to calculate the ratio of mercury-

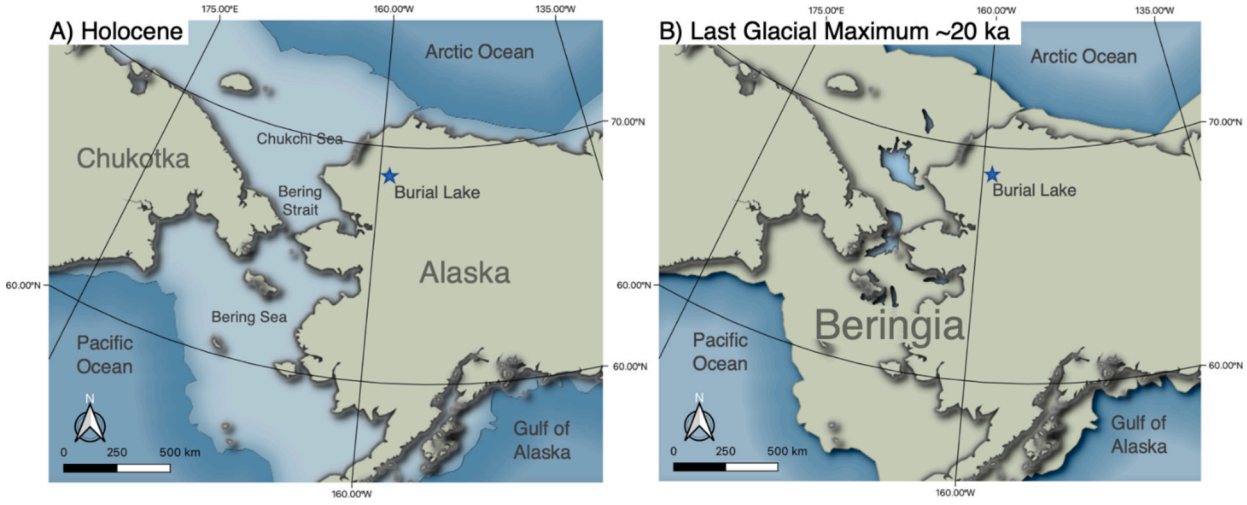

Fig. 1. A) Modern configuration of the Alaskan coastline and marginal seas. Burial Lake is situated in northwestern Alaska, on the northern slope of the western Brooks Range. B) Beringia during the Last Glacial Maximum (modified from Bond, 2019) when sea levels were ~ 130 m lower than today (Lambeck et al., 2014). By ~11 ka, rising sea levels flooded the Bering Land Bridge, allowing temperate water from the North Pacific to flow into the Arctic Ocean (Jakobsson et al., 2017). Between 11.5 and 9.5 ka, the advancing shoreline submerged ~65 % of the Bering Land Bridge, likely increasing maritime influences at Burial Lake, reducing seasonal temperature variability, and increasing precipitation (Gaglioti et al., 2017; Mann et al., 2001).

to-total organic carbon (Hg:C; Fig. 3E). Additionally, the mass sedimentation rate (g cm^{-2} yr^{-1}) was interpolated at 1 cm intervals for the top 25 cm of the surface core to align with Hg concentration measurements, enabling the calculation of Hg flux (Fig. 2C and D). All other reported values are derived from the original datasets.

3. Results and discussion

3.1. Climate warming and lake sediment mercury trends

High-latitude warming has been associated with environmental changes that enhance the atmospheric transport of Hg to polar regions and its subsequent deposition (Dastoor et al., 2022; Segato et al., 2023). An analysis of ice core Hg levels from the Greenland ice sheet identified a substantial rise in atmospheric Hg at the onset of the Holocene attributed to factors such as reduced sea ice, enhanced oceanic Hg evasion, and increased primary productivity (Segato et al., 2023). To explore how warming affected Hg dynamics at Burial Lake, Hg concentrations and flux were compared with Northern Hemisphere June and July insolation curves as proxies for large-scale temperature trends (Berger and Loutre, 1991; Erb et al., 2022; Laskar et al., 2004; Fig. 2A, C and D). Additionally, Hg trends were compared to the Burial Lake chironomid-inferred July mean air temperature record (T_{chiro}; Kurek et al., 2009; Fig. 2B). This proxy for regional midsummer temperatures is likely most relevant to processes, such as permafrost thaw and erosion, that are influenced by localized warming trends and mobilize Hg stored in frozen soils and sediments.

During the LGM, summer insolation in the northern high latitudes reached a minimum, and the T_{chiro} record from Burial Lake suggests that midsummer temperatures were ~3.5 °C cooler than today (Kurek et al., 2009; Laskar et al., 2004; Fig. 2A and B). Throughout this period, Hg concentrations remained relatively low, averaging 63 ± 4 μg/kg (n = 51; Fig. 2C). At 17.6 ka, T_{chiro} began to rise, reaching modern levels between ~14 and 10 ka, while Hg concentrations increased to 101.2 μg/kg at 14.1 ka, broadly synchronous with peak June insolation and elevated T_{chiro}.

Mercury concentrations subsequently decrease and fluctuate, while a maximum T_{chiro} of 11.0 °C occurs at 12.7 ka, exceeding modern temperatures (Kurek et al., 2009; Fig. 2B and C). Midsummer temperatures then cooled by ~1 °C, followed by an abrupt Hg concentration increase at 11.1 ka to 140.3 μg/kg, coinciding with maximum July insolation (Kurek et al., 2009; Laskar et al., 2004; Fig. 2A). After 10.6 ka, Hg concentrations gradually declined, roughly trending with decreasing June insolation until 4.8 ka, when Hg concentrations began to rise again.

In contrast, the Hg flux trend does not align with the June or July insolation trends or T_{chiro} values (Fig. 2A, B, and D). Mercury flux is elevated during the LGM but decreases until 16 ka, with values ranging from 13.7 to 3.6 μg m^{-2} yr^{-1}. Between ~17 and 15 ka, a minor

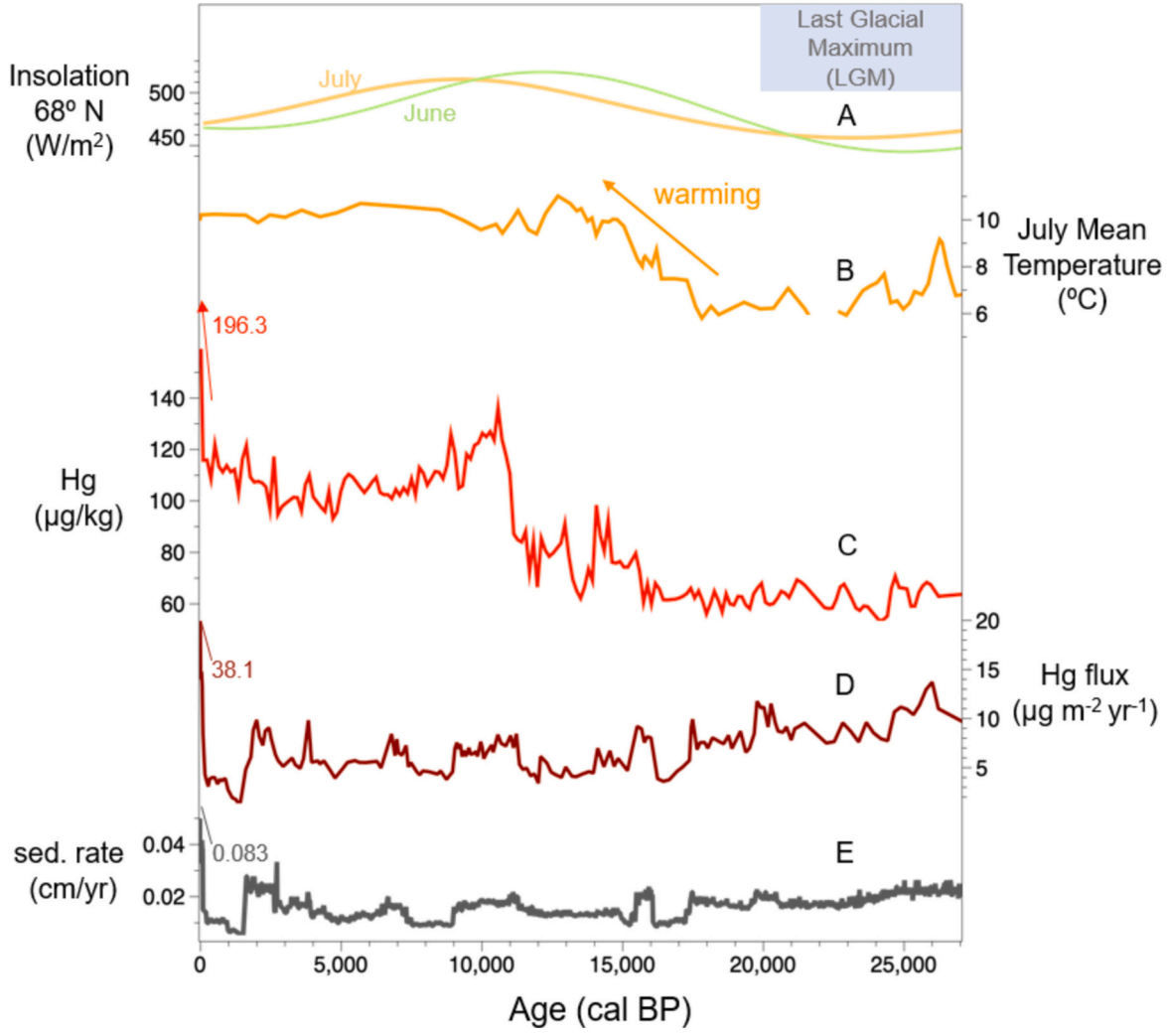

Fig. 2. Comparison of A) Mean June (21 May–20 June) and July insolation (21 June–20 July) at 68°N (Laskar et al., 2004), B) July mean air temperature reconstructed using chironomid species assemblage from Burial Lake (Kurek et al., 2009), C) total lake sediment mercury (Hg) concentration, D) mercury accumulation rate (Hg Flux), and E) sedimentation rate, calculated using contiguous ages and depths from the age-depth model.

radiocarbon age reversal introduces uncertainty into the age model, limiting sedimentation rate and Hg flux estimates during this period (SI Fig. S2 and Table S1, Fig. 2D and E). After 15 ka, the sedimentation rate stabilizes, and Hg flux remains relatively consistent, averaging 5.3 ± 1.3 μg m^{-2} yr^{-1} ($n = 25$) until 11.0 ka, with no apparent relationship to rising summer insolation or T_{chiro} trends.

Over the 27-ka record, Hg flux and sedimentation rates fluctuate in tandem and strongly correlate ($r = 0.87$; Fig. 2D and E; SI Fig. S3). Mercury flux is also positively correlated with dry bulk density (BD), which decreased from 1.0 to 0.2 g/cm^3 over the long-term ($r = 0.70$; SI Figs. S3 and S5D). Hence, the disconnect between Hg flux and warming trends suggests that atmospheric deposition or warming-driven processes were not the primary influences on lake sediment Hg accumulation rates. Rather, elevated Hg flux during the LGM likely reflects increased minerogenic Hg inputs, consistent with low TOC (Fig. 3B) and high sediment BD.

The long-term Hg concentration trend generally tracks summer insolation and T_{chiro} trends (Fig. 2A-C). The roughly synchronous rise in Hg concentrations and T_{chiro} values, alongside increasing insolation and their subsequent decline during the early to middle Holocene, suggests that regional midsummer temperatures and insolation influenced Hg concentrations over the long term. However, between 17.0 and 9.0 ka, Hg concentrations remain relatively tempered compared to the notable increases in both $T_{chiro,}$ and insolation trends, suggesting other factors influenced Hg concentrations during this time.

The absence of coinciding trends between Hg flux, summer insolation, and temperature (Fig. 2A, B, and D) suggests that mechanisms typically associated with warming, such as increased atmospheric deposition, erosion, or permafrost thaw, were not the primary drivers of Hg inputs to Burial Lake. Despite the summer warming trend after 16 ka, which might be expected to enhance Hg flux, the record shows relatively steady and lower Hg flux compared to LGM levels. Hence, the overall increase in Hg concentrations, decreasing Hg flux and BD, are likely driven by changes in sediment composition, such as increasing TOC, possibly resulting from greater transport of terrestrial OM to the lake (Fig. 2C; SI Fig. S5D; Fig. 3B).

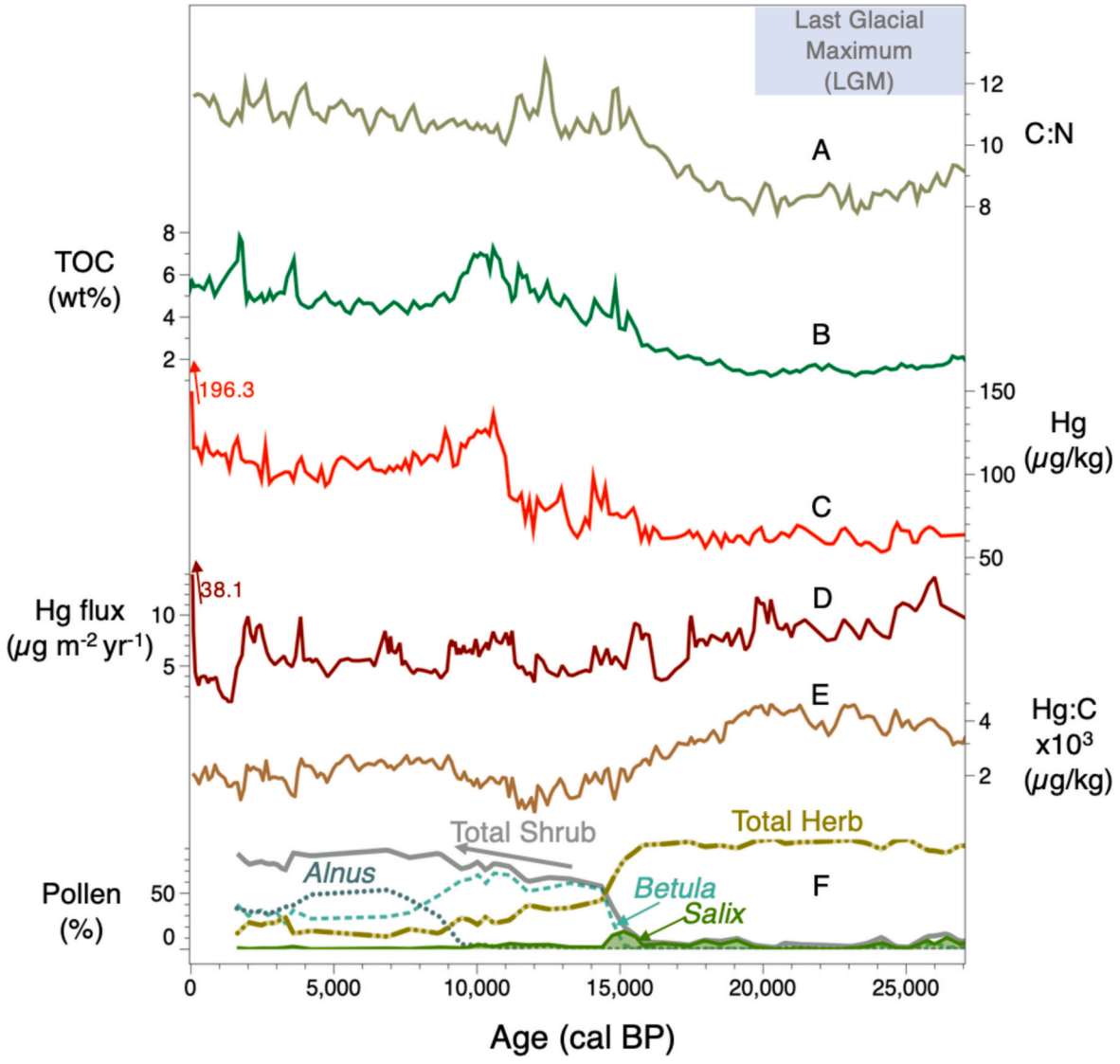

Fig. 3. Comparison of A) total organic carbon-to-nitrogen (C:N) mass ratio (Finkenbinder et al., 2015), B) lake sediment weight percent of total organic carbon (TOC; Finkenbinder et al., 2015), C) total lake sediment mercury (Hg) concentration, D) mercury accumulation rate (Hg Flux), E) mercury-to-total organic carbon ratio (Hg:C), and F) Total Shrub and Total Herb reflecting the combined percentages of pollen abundance from taxa in each respective group from the Burial Lake pollen record (Abbott et al., 2010). Total Shrub abundance includes *Alnus* (alder), *Betula* (birch), and *Salix* (willow) abundances which are also plotted separately here (Abbott et al., 2010).

3.2. Shrub tundra expansion and mercury dynamics

The ecosystem in the Burial Lake region during the LGM is characterized by a cold, dry, and sparsely vegetated tundra, with graminoids and forbs comprising the majority of the 'Total Herb' percent abundance in the pollen record (Fig. 3F; Abbott et al., 2010; Finkenbinder et al., 2015). The establishment of a shrub-dominated ecosystem (Total Shrub) begins with a brief *Salix* (shrub willow) peak at 15.2 ka, followed by the *Betula* (shrub birch) rise at 14.8 ka. This ecosystem shift is consistent with pollen records from other sites in northern Alaska (Anderson et al., 2004).

Mercury in Arctic tundra soils originates primarily from gaseous atmospheric Hg (Obrist et al., 2017). This process is driven by the uptake of elemental mercury (Hg(0)) by vegetation, which is subsequently oxidized to Hg(II) and incorporated into the soil as vegetation decomposes (Obrist et al., 2017; Zhou et al., 2021). Hence, the terrestrial Hg cycle in the Arctic is closely connected to the biogeochemical cycling of OM, which is influenced by vegetation type and ecosystem structure (Obrist et al., 2017; Schaefer et al., 2020; Zhou et al., 2021).

During the LGM, TOC remained low and stable, averaging 1.7 ± 0.3 % (n = 53), before beginning to increase after 17.0 ka (Fig. 3B). This upward trend continues, with fluctuations intensifying after 15.7 ka, coinciding with the transition to shrub tundra and reaching a peak of 8.0 % by 10.4 ka (Fig. 3F). Total organic carbon levels then decrease sharply to 4.9 % at 9.2 ka before stabilizing at more than twice the average LGM level, 4.5 ± 0.2 % (n = 49) until 5.0 ka. Subsequently, TOC becomes more variable with notable peaks at 3.6 and 1.7 ka and an average concentration of 5.4 ± 0.8 % (n = 40). Mercury concentrations strongly correlate with lake sediment TOC over the long term (r = 0.80; SI Fig. S3; Fig. 3C) and between 17.0 and 9.0 ka (r = 0.75; SI Fig. S4). In contrast, Hg flux (Fig. 3D) exhibits a moderate negative correlation with TOC over the 27-ka record (r = −0.59) and no significant correlation during the 17.0–9.0 ka interval.

Like the TOC trend, Hg concentrations begin to increase at 15.7 ka, roughly coinciding with the emergence of the shrub tundra ecosystem, while Hg flux remains relatively low and stable during this period

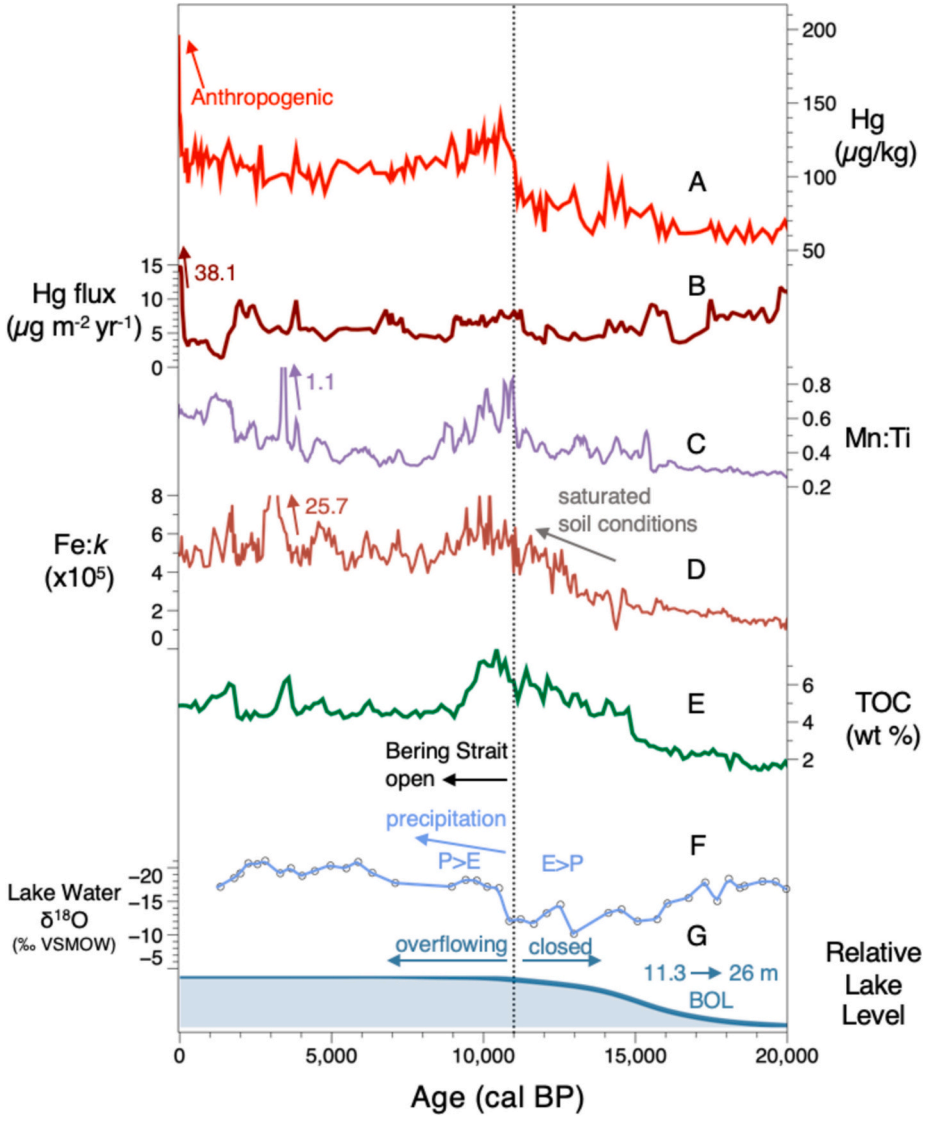

Fig. 4. A) Total mercury (Hg) concentration, B) mercury accumulation rate (Hg Flux), C) scanning X-ray fluorescence (XRF)-based manganese-to-titanium (Mn:Ti) ratio smoothed using 5-point moving average, D) XRF-based, iron-to-magnetic susceptibility (Fe:k) ratio, smoothed using a 5-point moving average, E) lake sediment weight percent of total organic carbon (TOC; Finkenbinder et al., 2015), F) chironomid lake water $\delta^{18}O$ composition where evaporation exceeds precipitation E > P between ~16 ka to 11 ka and precipitation exceeds evaporation P > E after ~11 ka (King et al., 2022), and G) Burial Lake relative lake level curve illustrating meters below overflow level (BOL; Finkenbinder et al., 2015). The dashed black line marks the estimated timing of the opening of the Bering Strait at ~11 ka (Jakobsson et al., 2017).

(Fig. 3B–D, F). However, these trends decouple between 14.1 and 11.0 ka, with Hg concentrations increasing but remaining low and highly variable, whereas TOC rises steadily. This decoupling suggests that factors such as changes in OM characteristics and soil properties influenced Hg concentrations during this time. At 11.0 ka, Hg concentrations show an abrupt increase that coincides with peak TOC levels but does not align with changes in taxon-specific pollen abundances, indicating that this increase was not caused by a shift in vegetation assemblage.

A more detailed understanding of the effects of vegetation change on OM characteristics and Hg concentrations might be gleaned by examining trends related to the Hg:C and C:N ratios (Fig. 3A, C and E). In Arctic regions, Hg:C ratios generally increase with depth in the soil profile, with the highest ratios observed in more decomposed OM and mineral soils (Lim et al., 2020; Olson et al., 2018). In the Burial Lake record, the highest Hg:C ratios, averaging $4.1 \pm 0.5 \times 10^3$ μg/kg ($n = 74$), occur before 19 ka, when the TOC and C:N ratios are relatively low (Fig. 3B). This further supports the interpretation that Hg deposited in the lake during this time was likely predominantly derived from mineral soils.

After 19 ka, Hg:C ratios begin to decline as C:N ratios and TOC levels rise (Fig. 3A, B, and E; Finkenbinder et al., 2015). An increasing contribution of terrestrial OM to the lake sediments is indicated by C:N ratios >10 after 16.2 ka, rising TOC levels, and the transition to shrub tundra around ~15 ka (Fig. 3F; Abbott et al., 2010; Finkenbinder et al., 2015; Meyers and Teranes, 2002). Between 15.0 and 9.5 ka, the lowest Hg:C ratios, averaging $1.7 \pm 0.2 \times 10^3$ μg/kg ($n = 50$), correspond with peak C:N ratios between 14.8 and 11.5 ka. Elevated C:N ratios can suggest less decomposed and potentially younger terrestrial OM, while low Hg:C ratios are consistent with fresher organic soils (Lim et al., 2020; Obrist et al., 2011; Olson et al., 2018).

The combination of elevated but variable Hg concentrations, relatively stable Hg flux, low Hg:C ratios, rising TOC and peak C:N ratios (Fig. 3A–E) suggests that the establishment of woody vegetation altered soil structure and OM characteristics in the catchment. Studies from temperate forests suggest that differences in plant litter types, including their lignin content and decomposition rates, influence Hg sorption and retention in soils (Pokharel and Obrist, 2011). Additionally, soils enriched with fulvic and humic acids are associated with more stable binding sites, enhancing Hg sequestration (Burns et al., 2014; Pokharel and Obrist, 2011). Furthermore, in Arctic regions, 'shrubification' has been linked to changes in factors affecting soil structure, including moisture, temperature, active layer depth, and decomposition rates (Frost et al., 2018; Mekonnen et al., 2021).

In some Arctic lakes, aquatic productivity may contribute to sediment Hg levels by facilitating the sequestration of Hg from the water column through binding to autochthonous OM (Galloway et al., 2024; Kirk et al., 2011; Outridge et al., 2007). Although a comprehensive analysis of aquatic productivity proxies was not conducted for Burial Lake, biogenic silica (BSi), a proxy for diatom productivity, was examined in previous studies (Finkenbinder et al., 2018, 2015; SI Fig. S5C). Biogenic silica correlates strongly with Hg concentrations over the 27-ka record ($r = 0.79$; SI Fig. S3 and Fig. S5B) but negatively correlates with Hg flux ($r = -0.56$; SI Fig. S3 and Fig. S5E). Additionally, between 17.0 and 9.0 ka, BSi exhibits a weak positive correlation with Hg concentrations ($r = 0.49$; SI Fig. S4) and has no significant relationship with Hg flux. Moreover, substantial fluctuations in the BSi and Hg concentration records do not coincide, suggesting that aquatic productivity does not strongly influence Hg levels in Burial Lake sediments. This is consistent with findings from a study in the central Northwest Territories, Canada, which found that the relationship between aquatic productivity and lake sediment Hg levels is less significant in lakes situated in shrub tundra regions (Galloway et al., 2024).

Following the transition to a shrub tundra-dominated ecosystem at ~15 ka, Hg flux remained relatively stable, while Hg concentrations moderately increased and fluctuated (Fig. 3C, D, and F). Although Hg concentrations strongly correlate with TOC over the long term, they decoupled from TOC trends between ~14 and 11 ka (Fig. 3B). During this period, TOC increased rapidly and consistently, C:N ratios peaked, and Hg:C ratios remained relatively low (Fig. 3A and E). The stability of Hg flux, despite changes in vegetation and OM characteristics, indicates that the establishment of shrub tundra did not noticeably impact the overall rate of Hg release from the catchment. However, these trends suggest that the greater abundance of woody taxa altered catchment soil properties and OM characteristics, modifying the association of Hg with OM and ultimately affecting Hg concentrations in lake sediments. These findings illustrate how vegetation type can influence the characteristics of terrestrial OM, lake sediment composition, and Hg mobilization in Arctic watersheds, underscoring the need for further investigation to better understand these processes.

3.3. Precipitation and mercury mobilization

During the LGM, sea levels were ~ 130 m lower (Lambeck et al., 2014), and the Bering and Chukchi Sea continental shelves were fully exposed (Fig. 1 B). This extended the distance between Burial Lake and major moisture sources, including the North Pacific and Arctic Oceans, limiting regional precipitation (Gaglioti et al., 2017; Mann et al., 2001). At Burial Lake, hydroclimate variability is recorded in lake levels and chironomid-inferred lake water $\delta^{18}O$ composition, which reflect regional shifts in moisture balance driven by broader climate changes (Fig. 4F and G). Core-transect data suggests that lake levels were low during the LGM, reaching <11.3 m below overflow levels and beginning to rise at 19.8 ka (Finkenbinder et al., 2015).

Chironomid-inferred lake water $\delta^{18}O$ values serve as a proxy for water balance expressed as precipitation minus evaporation (P − E), capturing changes in precipitation sources, temperature, and humidity (King et al., 2022; Fig. 4F). Between 20.0 and 16.0 ka, average lake water $\delta^{18}O$ values of −16.5 ‰ are consistent with a shallow, hydrologically closed lake with overall moisture deficits (King et al., 2022; Fig. 4G). Additionally, lower estimated precipitation $\delta^{18}O$ values are attributed to cooler atmospheric and sea surface temperatures (SSTs) in the Northeastern Pacific Ocean (King et al., 2022; Praetorius et al., 2020; SI Fig. S5A). From 16.0 to 12.9 ka, rising lake levels indicate increasing moisture availability, though conditions were likely variable (Finkenbinder et al., 2015). Increasing lake water $\delta^{18}O$ values align with rapid summer warming, while lower P − E values suggest overall drier conditions relative to today (King et al., 2022). Between 12.9 and 11.0 ka, precipitation $\delta^{18}O$ values sharply decreased, indicating drier conditions that are again consistent with cooler SST in the Northeastern Pacific (King et al., 2022; Praetorius et al., 2020).

During the late Pleistocene, spring thaw was probably the main annual hydrological event at Burial Lake, as it is in many Arctic regions today (Beel et al., 2021). Following an abrupt increase in SST at ~12.0 ka, a rapid 4.6 ‰ reduction in $\delta^{18}O$ values occurred at ~11 ka (SI Fig. S5A; Fig. 4F; King et al., 2022; Praetorius et al., 2020). This drastic shift coincides with the onset of an overflowing lake system and an increase in effective moisture ascribed to the establishment of a hydrological regime resembling modern conditions (Finkenbinder et al., 2015; King et al., 2022; Fig. 4G). This change was likely influenced by processes that enhance moisture transport to the Alaskan interior, including sea level rise, elevated SSTs, the opening of the Bering Strait, and alterations in the atmospheric and oceanic circulation patterns in the North Pacific (Bartlein et al., 2015; King et al., 2022). Today, meteorological data indicate that most precipitation at Burial Lake occurs as summer rainfall (Finkenbinder et al., 2015; King et al., 2022).

In continuous permafrost landscapes, drainage is limited by the impermeable frozen ground (Fig. 5A). The thawing of ice-rich permafrost, combined with summer precipitation, elevates soil moisture levels, leading to ponding and deepening of the active layer (Herndon et al., 2020; Fig. 5B). Prolonged soil saturation slows OM decomposition rates, resulting in the accumulation of a thick, organic-rich layer (Jorgenson et al., 2001). These factors can also cause fluctuations in pH and redox

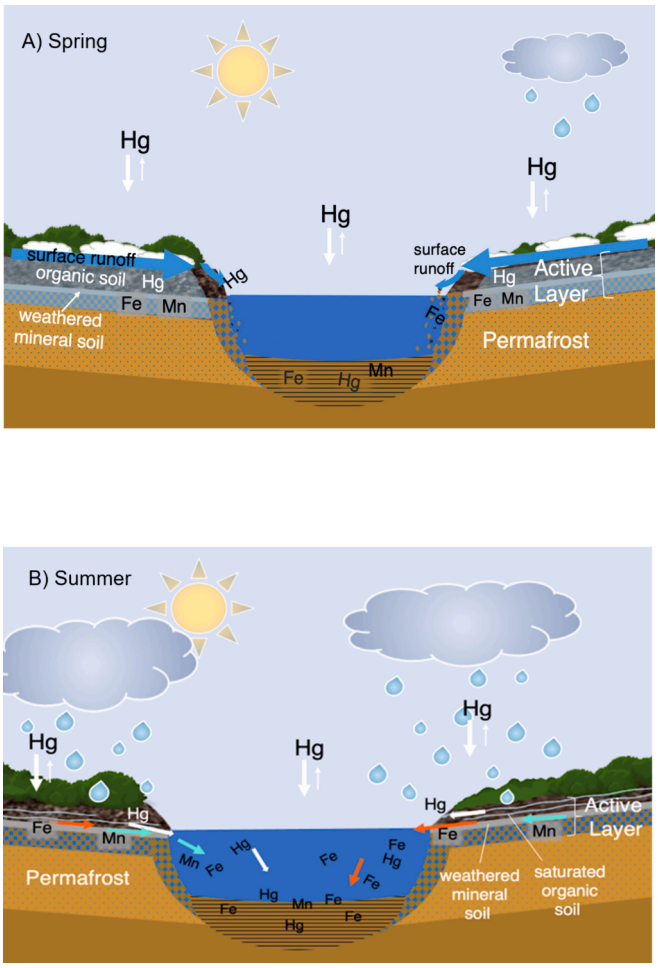

Fig. 5. A conceptual model illustrating seasonal mercury (Hg) transport changes in the Burial Lake watershed. A) During the spring, when the active layer is frozen, Hg associated with materials at the soil surface is transported by snowmelt and overland flow.
B) In summer, the active layer deepens, increasing storage capacity. Summer rain events and the thawing active layer raise perched water table levels in the catchment, enhancing the transport of materials, including Hg, to the lake through subsurface flow. Prolonged periods of saturated soil conditions lead to reducing conditions in the soil, mobilizing redox-sensitive metals, including iron (Fe) and manganese (Mn; Herndon et al., 2017).

conditions, which influence the mobility and transformations of redox-sensitive metals, including Hg, iron (Fe), and manganese (Mn), which readily complex with DOM in organic-rich soils (Branfireun et al., 2020; Gabriel and Williamson, 2004; Herndon et al., 2017; Pokrovsky et al., 2016b, 2016a; Poulin et al., 2019). The presence of iron-rich seeps along Burial Lake's shoreline provides evidence of ongoing chemical weathering and reductive dissolution of Fe in the catchment soils today (Hudson et al., 2022; SI Fig. S6A and B).

Proxies commonly used to identify reducing conditions in bottom waters or at the sediment-water interface include the manganese-to-titanium ratio (Mn:Ti) derived from X-ray fluorescence (XRF) as well as the ratio of iron (derived from XRF) to magnetic susceptibility (Fe:*k*; Croudace and Rothwell, 2015). However, in the Burial Lake sediment record, there is no evidence of post-depositional diagenetic alteration of Fe or Mn resulting from prolonged anoxic bottom waters (Abbott et al., 2010; Dorfman et al., 2015). This is supported by strong positive correlations over the long-term 27-ka record, including Fe:*k* ($r = 0.88$; SI Fig. S3) and Mn:Ti ($r = 0.77$) with Hg concentrations, as well as Fe:*k* ($r = 0.79$) and Mn:Ti ($r = 0.81$) with TOC. These relationships suggest that Fe and Mn were not remobilized in the lake sediments post-deposition but instead reflect inputs from the catchment. We thus propose that the saturated organic soils in the lake catchment are the primary source of diagenetic Fe and Mn deposited in the lake.

Rising Fe:*k* and Mn:Ti ratios beginning after 15.5 ka (Fig. 4C and D) suggest increasing chemical weathering in the lake catchment in response to saturated soil conditions (Fig. 5B; SI Fig. S7). Heightened Mn:Ti ratios are attributed to the preferential mobilization of Mn to the lake sediments, as Mn is more susceptible to chemical weathering and reductive dissolution than the relatively inert Ti (Croudace and Rothwell, 2015). Likewise, elevated Fe:*k* ratios signify an increase in the deposition of non- or weakly magnetic forms of Fe, such as hematite and other Fe(III) (oxyhydr)oxides formed by the weathering of Fe-bearing minerals in saturated catchment soils (Dorfman et al., 2015; Herndon et al., 2017). Therefore, this record provides the first insights into the timing and climate conditions related to the post-glacial development of iron-rich, waterlogged tundra soils commonly found throughout Alaska today (Barker et al., 2023; Emerson et al., 2015; Herndon et al., 2017; Hudson et al., 2022; Lipson et al., 2010; O'Donnell et al., 2024; Patzner et al., 2022).

The rapid increase in lake sediment Hg concentrations (a rise of 59 μg/kg over 500 years between 11.1 and 10.6 ka) and a 32 % rise in Hg flux, averaging 7.0 ± 0.7 μg m^{-2} yr^{-1} ($n = 26$) between 11.0 and 9.0 ka (Fig. 4A and B), are likely associated with increased precipitation during summer or early autumn. Between 17.0 and 9.0 ka, Fe:*k* ($r = 0.87$; SI Fig. S4) and Mn:Ti ($r = 0.82$) strongly correlate with Hg concentrations. Additionally, Fe:*k* ($r = 0.78$) and Mn:Ti ($r = 0.77$) show strong correlations with TOC. Peaks in TOC at 10.4 ka, Mn:Ti at 11.0 ka, and Fe:*k* at 10.0 ka (Fig. 4C–E) are roughly coeval with the rapid increase in Hg concentrations and the rise in Hg flux, further illustrating the synchronicity of these trends. These relationships suggest that the deepening active layer and increased hydrological connectivity facilitated the mobilization of dissolved materials, including Fe, Mn, and Hg, which were likely complexed with DOM and transported to the lake (Fig. 5B; SI Fig. S7).

In continuous permafrost regions, concentrations of soluble inorganic ions and reduced forms of Fe and Mn tend to increase with depth in the active layer (Barker et al., 2023, 2014; Herndon et al., 2017, 2015; Lafrenière and Lamoureux, 2019). During the late thaw season, intense or frequent rainfall events can flush these materials into surface waters via deep active layer flow paths (Barker et al., 2023, 2014; Herndon et al., 2017, 2015; Tashiro et al., 2020; Fig. 5B). The presence of a perched water table above the permafrost layer likely sustained saturated soil conditions, which enhanced the lateral transport of dissolved metals and OM (SI Fig. S7). As dissolved metals interact with DOM, they form stable colloidal complexes that can undergo coagulation and aggregation, transforming into larger particulate matter as they are transported to surface waters (Pokrovsky et al., 2016b, 2016a). The accumulation of these colloids and aggregates in the iron-rich seeps at Burial Lake suggests that these processes are taking place today (SI Fig. S6A and B).

The hydroclimate shift at ~11 ka marks the final well-characterized, major climate-driven change impacting the region since the LGM (Finkenbinder et al., 2015; King et al., 2022; Kurek et al., 2009). During the Holocene, insolation in the Northern Hemisphere gradually decreased (Berger and Loutre, 1991; Laskar et al., 2004; Fig. 2A), while local temperatures at Burial Lake stabilized (Kurek et al., 2009; Fig. 2B), likely due to rising sea levels in the early Holocene (Jakobsson et al., 2017; Lambeck et al., 2014; Praetorius et al., 2020). These sea level changes brought the shoreline closer to the study site, reducing interannual temperature variability through a stronger maritime influence (Fig. 1A and B). The establishment of shrub tundra dominance in the region after ~15 ka, followed by the expansion of *Alnus* at ~9 ka, marks the development of a stable ecosystem identified as moist shrub tundra, as evidenced by the relatively consistent pollen assemblage throughout the remainder of the Holocene (Abbott et al., 2010; Finkenbinder et al., 2015; Fig. 3F). After ~11 ka, stable high lake levels (Finkenbinder et al.,

2015; Fig. 4G) and relatively consistent $\delta^{18}O$ values (King et al., 2022; Fig. 4F) suggest that the local hydroclimate remained generally stable. Thus, variability in proxies, including Hg concentrations and flux, throughout the remainder of the Holocene may reflect the impacts of short-term climate fluctuations or localized environmental changes, such as modulations in the timing, intensity, or seasonality of precipitation, changes in catchment hydrology, or wildfires.

3.4. Comparison with similar studies

There is little consistency in research approaches and interpretations among comparable studies using long-term Hg records from Arctic and periglacial regions. Elevated sediment Hg concentrations in Lake CF3 on Baffin Island roughly coincided with increased OM during the early Holocene (Cooke et al., 2012). However, this study primarily focused on investigating the relationship between aquatic productivity and sediment Hg levels and did not examine catchment-related processes (Cooke et al., 2012). Mercury concentrations in the Lake CF8 record aligned with OM and metals such as Fe, Mn, Ti, copper (Cu), and zinc (Zn), a trend attributed to heightened catchment erosion (Wilson et al., 2012). Furthermore, the increased Hg concentrations and accumulation rates in the Andean alpine lake, Laguna de Los Anteojos, are attributed to changes in atmospheric deposition rates rather than catchment processes (Schneider et al., 2020).

Compared to the aforementioned studies, the interpretations of the Lake Hambre Hg record, despite being from a relatively organic-rich lake located in the Magellanic subpolar forest ecozone (Hermanns et al., 2013; Hermanns and Biester, 2013), are most similar to the Burial Lake findings. In the Lake Hambre sediment record, Hg concentrations increase toward the top of the core, and although Hg flux fluctuates, it remains relatively stable over the long term (Hermanns and Biester, 2013). Covariation among Hg, copper (Cu), and yttrium (Y) fluxes and concentrations is observed throughout this record, with elevated levels attributed to periods of increased precipitation, which likely leached these metals, complexed with dissolved or particulate OM, from catchment soils (Hermanns and Biester, 2013). Hence, consistent with our interpretations from the Burial Lake record, this study suggests that elevated lake sediment Hg concentrations and flux may be related to increased precipitation and the complexation of Hg with OM mobilized from catchment soils (Hermanns and Biester, 2013).

These studies emphasize the importance of atmospheric deposition, catchment processes, and the role of OM in influencing Hg dynamics in diverse permafrost and periglacial environments. However, to enable meaningful comparisons between studies, a more standardized approach to investigating the mechanisms driving Hg mobilization and deposition in these environments is warranted.

3.5. Modern implications

In the Burial Lake record, an anomalously low sedimentation rate and Hg flux are observed between 350 and 1800 CE (1.6 and 0.15 ka; Fig. 2D and E) and are attributed to poor age control within the 5–45 cm depth range of the A-10 surface core, owing to the lack of terrestrial macrofossils necessary for radiocarbon dating (Fig. S2 and Table S1). Therefore, we calculated the average Hg concentrations, flux, and sedimentation rate from 6.0 and 1.6 ka to establish natural background levels. The average Hg flux (6.3 ± 1.7 μg m^{-2} yr^{-1}, $n = 28$) from this time period yielded an estimate comparable to the preindustrial Hg flux (between ~2 and 10 μg m^{-2} yr^{-1}), measured in five lakes from Alaska's North Slope (Fitzgerald et al., 2005), and the focus factor corrected mean preindustrial flux (6.6 μg m^{-2} yr^{-1}) from eighteen Canadian Arctic lakes (65–83°N; Muir et al., 2009). Over the past century, the Burial Lake Hg flux rose abruptly, reaching a maximum of 38.1 μg m^{-2} yr^{-1} by ~1990 CE, roughly six times background levels. In comparison, Hg flux in the North Slope lake records increased by a factor of 2.5 relative to average levels from 1800 to 1850 CE (Fitzgerald et al., 2005).

Mercury concentrations in Burial Lake sediments also increased drastically, peaking at 196.3 μg/kg in 1990 CE, 88 % above the background average of 104.4 ± 8.2 μg/kg ($n = 45$; Fig. 2 C). Furthermore, sedimentation rates during this period increased substantially, reaching 0.083 cm/yr, nearly five times the background rate of 0.017 ± 0.005 cm/yr (Fig. 2 E). Such increases in sedimentation rates are commonly observed in modern Arctic lake sediments and are thought to be driven by climate-related factors, such as intensified erosion, higher precipitation, and permafrost thaw (Cooke et al., 2012; Fitzgerald et al., 2005; Muir et al., 2009; St. Pierre et al., 2019; Zhang et al., 2022).

Anthropogenic emissions have resulted in a 7.5-fold enrichment of atmospheric Hg compared to natural background levels before 2000 BCE (Amos et al., 2013). This enrichment is supported by Hg records from remote peatlands and lake sediments, which show a three- to fivefold rise in Hg deposition compared to the preindustrial era (Streets et al., 2017). Hence, the modern rise in Hg levels in Burial Lake sediments may be influenced by several factors including increased atmospheric Hg, a 2–3 °C rise in the Arctic temperatures since the late 19th century (Post et al., 2019), a ~17 % increase in Alaska's precipitation over the past seven decades (Wendler et al., 2017), and widespread 'shrubification' or greening north of treeline (Heijmans et al., 2022). However, further studies are needed to quantify and apportion the relative impacts of climate-driven processes and anthropogenic emissions to improve our understanding of the Hg cycle in permafrost regions.

4. Conclusion

The effects of summer temperature, vegetation, and precipitation on Hg dynamics in an Arctic lake catchment are interconnected and challenging to fully disentangle. However, distinct climate shifts recorded in the Burial Lake paleoclimate record offer a unique opportunity to evaluate how these changes influenced the Hg sediment record, with additional context provided by environmental proxies including Fe:*k*, Mn:Ti, Hg:C, and C:N ratios.

This study suggests that increased summer precipitation, resulting from a hydroclimate shift, had the most pronounced impact on lake sediment Hg levels. Between 11.0 and 9.0 ka, Hg flux remained elevated, increasing by 32 %, compared to relatively steady levels observed since 15 ka. During this period, Hg concentrations rose abruptly and remained elevated throughout the preindustrial Holocene, with average sediment concentrations (110.1 ± 9.9 μg/kg, $n = 87$) nearly double those observed during the LGM. This increase likely coincided with the development of a saturated, organic-rich active layer and enhanced hydrological connectivity, which may have facilitated the mobilization and transport of materials, including Hg, Fe, and Mn, complexed with OM, from catchment soils.

The overall increase in Hg concentrations in the Burial Lake record is attributed to long-term vegetation changes and warming. However, the simultaneous gradual decline in Hg flux reflects a change in sediment composition, with Hg becoming increasingly associated with OM rather than mineral matter after ~16 ka. Following the transition to shrub tundra after ~15 ka and as midsummer temperatures and insolation reached modern levels between ~14 and 10 ka, Hg concentrations exhibit minor and variable increases, while Hg flux remains low and stable. Trends in Fe:*k*, Mn:Ti, C:N, and Hg:C ratios during this period suggest that Hg dynamics were influenced by processes affecting active layer thickness, soil saturation, redox conditions, and OM decomposition rates. Furthermore, these processes are interconnected with the accumulation of organic-rich soils and their capacity to sequester or release Hg, highlighting the complex interactions between climate, vegetation, and Hg cycling in the Arctic.

By 1990 CE, relative to average background levels, modern Hg flux at Burial Lake had increased sixfold, while Hg concentrations rose by 88 %, likely driven by contributions from anthropogenic Hg emissions and climate change. These findings indicate a substantial rise in Hg released

from permafrost-affected soils compared to natural background levels. This study contributes to understanding the connections between climate change and the Arctic Hg cycle and identifies processes needing further research. Advancing our understanding of Hg dynamics in Arctic watersheds will improve our ability to evaluate risks and develop strategies to mitigate environmental and human health impacts.

CRediT authorship contribution statement

Melissa Griffore: Writing – review & editing, Writing – original draft, Methodology, Formal analysis, Data curation, Conceptualization. **Mark Abbott:** Writing – review & editing, Supervision, Funding acquisition, Data curation, Conceptualization. **Eitan Shelef:** Writing – review & editing, Supervision, Funding acquisition, Data curation, Conceptualization. **Matthew Finkenbinder:** Writing – review & editing, Data curation. **Joseph Stoner:** Writing – review & editing, Funding acquisition. **Mary Edwards:** Writing – review & editing.

Funding

Grants # NSF-ARC 0909545 to JS and MA and # 1841400 to ES and MA from the United States National Science Foundation (NSF).

Declaration of competing interest

The authors declare that they have no known competing financial interests or personal relationships that could have appeared to influence the work reported in this paper.

Appendix A. Supplementary data

Supplementary data to this article can be found online at https://doi.org/10.1016/j.scitotenv.2025.178440.

Data availability

Data is available here: 10.17632/zmy38p927p.1

References

Abbott, M.B., Stafford, T.W., 1996. Radiocarbon geochemistry of modern and ancient Arctic Lake systems, Baffin Island, Canada. Quat. Res. 45, 300–311. https://doi.org/10.1006/qres.1996.0031.

Abbott, M.B., Edwards, M.E., Finney, B.P., 2010. A 40,000-yr record of environmental change from burial Lake in Northwest Alaska. Quat. Res. 74, 156–165. https://doi.org/10.1016/j.yqres.2010.03.007.

Åkerblom, S., Meili, M., Bringmark, L., Johansson, K., Kleja, D.B., Bergkvist, B., 2008. Partitioning of hg between solid and dissolved organic matter in the humus layer of boreal forests. Water Air Soil Pollut. 189, 239–252. https://doi.org/10.1007/s11270-007-9571-1.

Amos, H.M., Jacob, D.J., Streets, D.G., Sunderland, E.M., 2013. Legacy impacts of all-time anthropogenic emissions on the global mercury cycle. Glob. Biogeochem. Cycles 27, 410–421. https://doi.org/10.1002/gbc.20040.

Anderson, P.M., Edwards, M.E., Brubaker, L.B., 2004. Results and paleoclimate implications of 35 years of paleoecological research in Alaska. In: Developments in Quaternary Sciences, the Quaternary Period in the United States. Elsevier, pp. 427–440. https://doi.org/10.1016/S1571-0866(03)01019-4.

Appleby, P.G., Oldfield, F., 1983. The assessment of 210Pb data from sites with varying sediment accumulation rates. Hydrobiologia 29–35. https://doi.org/10.1007/BF00028424.

Barker, A.J., Douglas, T.A., Jacobson, A.D., McClelland, J.W., Ilgen, A.G., Khosh, M.S., Lehn, G.O., Trainor, T.P., 2014. Late season mobilization of trace metals in two small Alaskan arctic watersheds as a proxy for landscape scale permafrost active layer dynamics. Chem. Geol. 381, 180–193. https://doi.org/10.1016/j.chemgeo.2014.05.012.

Barker, A.J., Sullivan, T.D., Baxter, W.B., Barbato, R.A., Gallaher, S., Patton, G.E., Smith, J.P., Douglas, T.A., 2023. Iron oxidation–reduction processes in warming permafrost soils and surface waters expose a seasonally rusting arctic watershed. ACS Earth Space Chem. 7, 1479–1495. https://doi.org/10.1021/acsearthspacechem.2c00367.

Barst, B.D., Chételat, J., Basu, N., 2022. Toxicological risk of mercury for fish and invertebrate prey in the Arctic. Sci. Total Environ. 836, 155702. https://doi.org/10.1016/j.scitotenv.2022.155702.

Bartlein, P.J., Edwards, M.E., Hostetler, S.W., Shafer, S.L., Anderson, P.M., Brubaker, L.B., Lozhkin, A.V., 2015. Early-Holocene warming in Beringia and its mediation by sea-level and vegetation changes. Clim. Past 11, 1197–1222. https://doi.org/10.5194/cp-11-1197-2015.

Beel, C.R., Heslop, J.K., Orwin, J.F., Pope, M.A., Schevers, A.J., Hung, J.K.Y., Lafrenière, M.J., Lamoureux, S.F., 2021. Emerging dominance of summer rainfall driving High Arctic terrestrial-aquatic connectivity. Nat. Commun. 12, 1448. https://doi.org/10.1038/s41467-021-21759-3.

Berger, A., Loutre, M.F., 1991. Insolation values for the climate of the last 10 million years. Quat. Sci. Rev. 10, 297–317. https://doi.org/10.1016/0277-3791(91)90033-Q.

Bintanja, R., 2018. The impact of Arctic warming on increased rainfall. Sci. Rep. 8, 16001. https://doi.org/10.1038/s41598-018-34450-3.

Biskaborn, B.K., Smith, S.L., Noetzli, J., Matthes, H., Vieira, G., Streletskiy, D.A., Schoeneich, P., Romanovsky, V.E., Lewkowicz, A.G., Abramov, A., Allard, M., Boike, J., Cable, W.L., Christiansen, H.H., Delaloye, R., Diekmann, B., Drozdov, D., Etzelmüller, B., Grosse, G., Guglielmin, M., Ingeman-Nielsen, T., Isaksen, K., Ishikawa, M., Johansson, M., Johannsson, H., Joo, A., Kaverin, D., Kholodov, A., Konstantinov, P., Kröger, T., Lambiel, C., Lanckman, J.-P., Luo, D., Malkova, G., Meiklejohn, I., Moskalenko, N., Oliva, M., Phillips, M., Ramos, M., Sannel, A.B.K., Sergeev, D., Seybold, C., Skryabin, P., Vasiliev, A., Wu, Q., Yoshikawa, K., Zheleznyak, M., Lantuit, H., 2019. Permafrost is warming at a global scale. Nat. Commun. 10, 264. https://doi.org/10.1038/s41467-018-08240-4.

Blaauw, M., Christen, J.A., 2011. Flexible paleoclimate age-depth models using an autoregressive gamma process. Bayesian Anal. 6. https://doi.org/10.1214/11-BA618.

Bond, J.D., 2019. Paleodrainage map of Beringia. Yukon Geological Survey. Open File 2019-2.

Branfireun, B.A., Cosio, C., Poulain, A.J., Riise, G., Bravo, A.G., 2020. Mercury cycling in freshwater systems - an updated conceptual model. Sci. Total Environ. 745, 140906. https://doi.org/10.1016/j.scitotenv.2020.140906.

Burke, S.M., Zimmerman, C.E., Branfireun, B.A., Koch, J.C., Swanson, H.K., 2018. Patterns and controls of mercury accumulation in sediments from three thermokarst lakes on the Arctic Coastal Plain of Alaska. Aquat. Sci. 80, 1. https://doi.org/10.1007/s00027-017-0553-0.

Burns, D.A., Woodruff, L.G., Bradley, P.M., Cannon, W.F., 2014. Mercury in the soil of two contrasting watersheds in the Eastern United States. PLoS One 9, e86855. https://doi.org/10.1371/journal.pone.0086855.

Cooke, C.A., Wolfe, A.P., Michelutti, N., Balcom, P.H., Briner, J.P., 2012. A Holocene perspective on algal mercury scavenging to sediments of an Arctic Lake. Environ. Sci. Technol. 46, 7135–7141. https://doi.org/10.1021/es3003124.

Croudace, I.W., Rothwell, R.G. (Eds.), 2015. Micro-XRF Studies of Sediment Cores: Applications of a Non-destructive Tool for the Environmental Sciences, Developments in Paleoenvironmental Research. Springer, Dordrecht.

Dastoor, A., Wilson, S.J., Travnikov, O., Ryjkov, A., Angot, H., Christensen, J.H., Steenhuisen, F., Muntean, M., 2022. Arctic atmospheric mercury: sources and changes. Sci. Total Environ. 839, 156213. https://doi.org/10.1016/j.scitotenv.2022.156213.

Dorfman, J.M., Stoner, J.S., Finkenbinder, M.S., Abbott, M.B., Xuan, C., St-Onge, G., 2015. A 37,000-year environmental magnetic record of aeolian dust deposition from Burial Lake, Arctic Alaska. Quat. Sci. Rev. 128, 81–97. https://doi.org/10.1016/j.quascirev.2015.08.018.

Emerson, D., Scott, J.J., Benes, J., Bowden, W.B., 2015. Microbial iron oxidation in the Arctic tundra and its implications for biogeochemical cycling. Appl. Environ. Microbiol. 81, 8066–8075. https://doi.org/10.1128/AEM.02832-15.

Erb, M.P., McKay, N.P., Steiger, N., Dee, S., Hancock, C., Ivanovic, R.F., Gregoire, L.J., Valdes, P., 2022. Reconstructing Holocene temperatures in time and space using paleoclimate data assimilation. Clim. Past 18, 2599–2629. https://doi.org/10.5194/cp-18-2599-2022.

Finkenbinder, M.S., Abbott, M.B., Finney, B.P., Stoner, J.S., Dorfman, J.M., 2015. A multi-proxy reconstruction of environmental change spanning the last 37,000 years from Burial Lake, Arctic Alaska. Quat. Sci. Rev. 126, 227–241. https://doi.org/10.1016/j.quascirev.2015.08.031.

Finkenbinder, M.S., Abbott, M.B., Stoner, J.S., Ortiz, J.D., Finney, B.P., Dorfman, J.M., Stansell, N.D., 2018. Millennial-scale variability in Holocene aquatic productivity from Burial Lake, Arctic Alaska. Quat. Sci. Rev. 187, 220–234. https://doi.org/10.1016/j.quascirev.2018.03.019.

Fitzgerald, W.F., Engstrom, D.R., Lamborg, C.H., Tseng, C.-M., Balcom, P.H., Hammerschmidt, C.R., 2005. Modern and historic atmospheric mercury fluxes in northern Alaska: global sources and Arctic depletion. Environ. Sci. Technol. 39, 557–568. https://doi.org/10.1021/es049128x.

Frost, G.V., Epstein, H.E., Walker, D.A., Matyshak, G., Ermokhina, K., 2018. Seasonal and long-term changes to active-layer temperatures after tall Shrubland expansion and succession in Arctic tundra. Ecosystems 21, 507–520. https://doi.org/10.1007/s10021-017-0165-5.

Gabriel, M.C., Williamson, D.G., 2004. Principal biogeochemical factors affecting the speciation and transport of mercury through the terrestrial environment. Environ. Geochem. Health 26, 421–434. https://doi.org/10.1007/s10653-004-1308-0.

Gaglioti, B.V., Mann, D.H., Wooller, M.J., Jones, B.M., Wiles, G.C., Groves, P., Kunz, M.L., Baughman, C.A., Reanier, R.E., 2017. Younger-Dryas cooling and sea-ice feedbacks were prominent features of the Pleistocene-Holocene transition in Arctic Alaska. Quat. Sci. Rev. 169, 330–343. https://doi.org/10.1016/j.quascirev.2017.05.012.

Galloway, J.M., Parsons, M.B., Ardakani, O.H., Falck, H., Fewster, R.E., Swindles, G.T., Sanei, H., Palmer, M.J., Nasser, N.A., Patterson, R.T., 2024. Organic matter is a predominant control on total mercury concentration of near-surface lake sediments

across a boreal to low Arctic tundra transect in northern Canada. Sci. Total Environ. 954, 176466. https://doi.org/10.1016/j.scitotenv.2024.176466.
Gordon, J., Quinton, W., Branfireun, B.A., Olefeldt, D., 2016. Mercury and methylmercury biogeochemistry in a thawing permafrost wetland complex, Northwest Territories, Canada. Hydrol. Process. 30, 3627–3638. https://doi.org/10.1002/hyp.10911.
Gudmundsson, L., Kirchner, J., Gädeke, A., Noetzli, J., Biskaborn, B.K., 2022. Attributing observed permafrost warming in the northern hemisphere to anthropogenic climate change. Environ. Res. Lett. 17, 095014. https://doi.org/10.1088/1748-9326/ac8ec2.
Hamilton, T.D., 2010. Surficial Geologic Map of the Noatak National Preserve, Alaska.
Heijmans, M.M.P.D., Magnússon, R.Í., Lara, M.J., Frost, G.V., Myers-Smith, I.H., van Huissteden, J., Jorgenson, M.T., Fedorov, A.N., Epstein, H.E., Lawrence, D.M., Limpens, J., 2022. Tundra vegetation change and impacts on permafrost. Nat. Rev. Earth Environ. 3, 68–84. https://doi.org/10.1038/s43017-021-00233-0.
Hermanns, Y.-M., Biester, H., 2013. A 17,300-year record of mercury accumulation in a pristine lake in southern Chile. J. Paleolimnol. 49, 547–561. https://doi.org/10.1007/s10933-012-9668-4.
Hermanns, Y.-M., Cortizas, A.M., Arz, H., Stein, R., Biester, H., 2013. Untangling the influence of in-lake productivity and terrestrial organic matter flux on 4,250 years of mercury accumulation in Lake Hambre, Southern Chile. J. Paleolimnol. 49, 563–573. https://doi.org/10.1007/s10933-012-9657-7.
Herndon, E.M., Yang, Z., Bargar, J., Janot, N., Regier, T.Z., Graham, D.E., Wullschleger, S.D., Gu, B., Liang, L., 2015. Geochemical drivers of organic matter decomposition in arctic tundra soils. Biogeochemistry 126, 397–414. https://doi.org/10.1007/s10533-015-0165-5.
Herndon, E., AlBashaireh, A., Singer, D., Roy Chowdhury, T., Gu, B., Graham, D., 2017. Influence of iron redox cycling on organo-mineral associations in Arctic tundra soil. Geochim. Cosmochim. Acta 207, 210–231. https://doi.org/10.1016/j.gca.2017.02.034.
Herndon, E., Kinsman-Costello, L., Godsey, S., 2020. Biogeochemical cycling of redox-sensitive elements in permafrost-affected ecosystems. In: Dontsova, K., Balogh-Brunstad, Z., Le Roux, G. (Eds.), Geophysical Monograph Series. Wiley, pp. 245–265. https://doi.org/10.1002/9781119413332.ch12.
Hudson, J.M., Michaud, A.B., Emerson, D., Chin, Y.-P., 2022. Spatial distribution and biogeochemistry of redox active species in arctic sedimentary porewaters and seeps. Environ Sci Process Impacts 24, 426–438. https://doi.org/10.1039/D1EM00505G.
Jakobsson, M., Pearce, C., Cronin, T.M., Backman, J., Anderson, L.G., Barrientos, N., Björk, G., Coxall, H., de Boer, A., Mayer, L.A., Mörth, C.-M., Nilsson, J., Rattray, J.E., Stranne, C., Semiletov, I., O'Regan, M., 2017. Post-glacial flooding of the Bering Land Bridge dated to 11 cal ka BP based on new geophysical and sediment records. Clim. Past 13, 991–1005. https://doi.org/10.5194/cp-13-991-2017.
Jonsson, S., Mastromonaco, M.N., Wang, F., Bravo, A.G., Cairns, W.R.L., Chételat, J., Douglas, T.A., Lescord, G., Ukonmaanaho, L., Heimbürger-Boavida, L.-E., 2022. Arctic methylmercury cycling. Sci. Total Environ. 850, 157445. https://doi.org/10.1016/j.scitotenv.2022.157445.
Jorgenson, M.T., Racine, C.H., Walters, J.C., Osterkamp, T.E., 2001. Permafrost degradation and ecological changes associated with a warmingclimate in central Alaska. Clim. Chang. 48, 551–579.
King, A.L., Anderson, L., Abbott, M., Edwards, M., Finkenbinder, M.S., Finney, B., Wooller, M.J., 2022. A stable isotope record of late quaternary hydrologic change in the northwestern Brooks Range, Alaska (eastern Beringia). J. Quat. Sci. 37, 928–943. https://doi.org/10.1002/jqs.3368.
Kirk, J.L., Muir, D.C.M., Antoniades, D., Douglas, M.S.V., Evans, M.S., Jackson, T.A., Kling, H., Lamoureux, S., Lim, D.S.S., Pienitz, R., Smol, J.P., Stewart, K., Wang, X., Yang, F., 2011. Climate change and mercury accumulation in Canadian high and subarctic lakes. Environ. Sci. Technol. 45, 964–970. https://doi.org/10.1021/es102840u.
Kurek, J., Cwynar, L.C., Ager, T.A., Abbott, M.B., Edwards, M.E., 2009. Late Quaternary paleoclimate of western Alaska inferred from fossil chironomids and its relation to vegetation histories. Quat. Sci. Rev. 28, 799–811. https://doi.org/10.1016/j.quascirev.2008.12.001.
Lafrenière, M.J., Lamoureux, S.F., 2019. Effects of changing permafrost conditions on hydrological processes and fluvial fluxes. Earth Sci. Rev. 191, 212–223. https://doi.org/10.1016/j.earscirev.2019.02.018.
Lambeck, K., Rouby, H., Purcell, A., Sun, Y., Sambridge, M., 2014. Sea level and global ice volumes from the Last Glacial Maximum to the Holocene. Proc. Natl. Acad. Sci. USA 111, 15296–15303. https://doi.org/10.1073/pnas.1411762111.
Laskar, J., Robutel, P., Joutel, F., Gastineau, M., Correia, A.C.M., Levrard, B., 2004. A long-term numerical solution for the insolation quantities of the Earth. A&A 428, 261–285. https://doi.org/10.1051/0004-6361:20041335.
Lim, A.G., Jiskra, M., Sonke, J.E., Loiko, S.V., Kosykh, N., Pokrovsky, O.S., 2020. A revised pan-Arctic permafrost soil Hg pool based on Western Siberian peat Hg and carbon observations. Biogeosciences 17, 3083–3097. https://doi.org/10.5194/bg-17-3083-2020.
Lipson, D.A., Jha, M., Raab, T.K., Oechel, W.C., 2010. Reduction of iron (III) and humic substances plays a major role in anaerobic respiration in an Arctic peat soil. J. Geophys. Res. 115, G00I06. https://doi.org/10.1029/2009JG001147.
Lora, J.M., Mitchell, J.L., Tripati, A.E., 2016. Abrupt reorganization of North Pacific and western North American climate during the last deglaciation. Geophys. Res. Lett. 43. https://doi.org/10.1002/2016GL071244.
Mann, D.H., Reanier, R.E., Peteet, D.M., Kunz, M.L., Johnson, M., 2001. Environmental change and arctic paleoindians. Arct. Anthropol. 119–138.
McCrystall, M.R., Stroeve, J., Serreze, M., Forbes, B.C., Screen, J.A., 2021. New climate models reveal faster and larger increases in Arctic precipitation than previously projected. Nat. Commun. 12, 6765. https://doi.org/10.1038/s41467-021-27031-y.
Mekonnen, Z.A., Riley, W.J., Berner, L.T., Bouskill, N.J., Torn, M.S., Iwahana, G., Breen, A.L., Myers-Smith, I.H., Criado, M.G., Liu, Y., Euskirchen, E.S., Goetz, S.J., Mack, M.C., Grant, R.F., 2021. Arctic tundra shrubification: a review of mechanisms and impacts on ecosystem carbon balance. Environ. Res. Lett. 16, 053001. https://doi.org/10.1088/1748-9326/abf28b.
Menne, Durre, I., Korzeniewski, B., McNeill, S., Thomas, K., Yin, X., Anthony, S., Ray, R., Vose, R.S., Gleason, B.E., Houston, T.G., 2012. Ivotuk Pass, AK meteorological station data USW00026564. [WWW document]. URL. https://www.ncdc.noaa.gov/cdo-web/datasets/GHCND/stations/GHCND:USW00026564/detail (accessed 5.19.24).
Meyers, P.A., Teranes, J.L., 2002. Sediment organic matter. In: Last, W.M., Smol, J.P. (Eds.), Tracking Environmental Change Using Lake Sediments, Developments in Paleoenvironmental Research. Kluwer Academic Publishers, Dordrecht, pp. 239–269. https://doi.org/10.1007/0-306-47670-3_9.
Mu, C., Schuster, Paul F., Abbott, Benjamin W., Kang, S., Guo, J., Sun, S., Wu, Q., Zhang, T., 2020. Permafrost degradation enhances the risk of mercury release on Qinghai-Tibetan Plateau. Sci. Total Environ. 708, 135127. https://doi.org/10.1016/j.scitotenv.2019.135127.
Muir, D.C.G., Wang, X., Yang, F., Nguyen, N., Jackson, T.A., Evans, M.S., Douglas, M., Köck, G., Lamoureux, S., Pienitz, R., Smol, J.P., Vincent, W.F., Dastoor, A., 2009. Spatial trends and historical deposition of mercury in eastern and northern Canada inferred from lake sediment cores. Environ. Sci. Technol. 43, 4802–4809. https://doi.org/10.1021/es8035412.
Obrist, D., Johnson, D.W., Lindberg, S.E., Luo, Y., Hararuk, O., Bracho, R., Battles, J.J., Dail, D.B., Edmonds, R.L., Monson, R.K., Ollinger, S.V., Pallardy, S.G., Pregitzer, K. S., Todd, D.E., 2011. Mercury distribution across 14 U.S. forests. Part I: spatial patterns of concentrations in biomass, litter, and soils. Environ. Sci. Technol. 45, 3974–3981. https://doi.org/10.1021/es104384m.
Obrist, D., Pearson, C., Webster, J., Kane, T., Lin, C.-J., Aiken, G.R., Alpers, C.N., 2016. A synthesis of terrestrial mercury in the western United States: spatial distribution defined by land cover and plant productivity. Sci. Total Environ. 568, 522–535. https://doi.org/10.1016/j.scitotenv.2015.11.104.
Obrist, D., Agnan, Y., Jiskra, M., Olson, C.L., Colegrove, D.P., Hueber, J., Moore, C.W., Sonke, J.E., Helmig, D., 2017. Tundra uptake of atmospheric elemental mercury drives Arctic mercury pollution. Nature 547, 201–204. https://doi.org/10.1038/nature22997.
O'Donnell, J.A., Carey, M.P., Koch, J.C., Baughman, C., Hill, K., Zimmerman, C.E., Sullivan, P.F., Dial, R., Lyons, T., Cooper, D.J., Poulin, B.A., 2024. Metal mobilization from thawing permafrost to aquatic ecosystems is driving rusting of Arctic streams. Commun. Earth Environ. 5, 268. https://doi.org/10.1038/s43247-024-01446-z.
Olson, C., Jiskra, M., Biester, H., Chow, J., Obrist, D., 2018. Mercury in active-layer tundra soils of Alaska: concentrations, pools, origins, and spatial distribution. Glob. Biogeochem. Cycles 32, 1058–1073. https://doi.org/10.1029/2017GB005840.
Olson, C.L., Jiskra, M., Sonke, J.E., Obrist, D., 2019. Mercury in tundra vegetation of Alaska: spatial and temporal dynamics and stable isotope patterns. Sci. Total Environ. 660, 1502–1512. https://doi.org/10.1016/j.scitotenv.2019.01.058.
Oswald, C.J., Branfireun, B.A., 2014. Antecedent moisture conditions control mercury and dissolved organic carbon concentration dynamics in a boreal headwater catchment. Water Resour. Res. 50, 6610–6627. https://doi.org/10.1002/2013WR014736.
Outridge, Sanei, H., Stern, Hamilton, Goodarzi, F., 2007. Evidence for control of mercury accumulation rates in Canadian High Arctic Lake sediments by variations of aquatic primary productivity. Environ. Sci. Technol. 41, 5259–5265. https://doi.org/10.1021/es070408x.
Pastick, N.J., Jorgenson, M.T., Wylie, B.K., Nield, S.J., Johnson, K.D., Finley, A.O., 2015. Distribution of near-surface permafrost in Alaska: estimates of present and future conditions. Remote Sens. Environ. 168, 301–315. https://doi.org/10.1016/j.rse.2015.07.019.
Patzner, M.S., Kainz, N., Lundin, E., Barczok, M., Smith, C., Herndon, E., Kinsman-Costello, L., Fischer, S., Straub, D., Kleindienst, S., Kappler, A., Bryce, C., 2022. Seasonal fluctuations in iron cycling in thawing permafrost peatlands. Environ. Sci. Technol. 56, 4620–4631. https://doi.org/10.1021/acs.est.1c06937.
Pokharel, A.K., Obrist, D., 2011. Fate of mercury in tree litter during decomposition. Biogeosciences 8, 2507–2521. https://doi.org/10.5194/bg-8-2507-2011.
Pokrovsky, O.S., Manasypov, R.M., Loiko, S.V., Krickov, I.A., Kopysov, S.G., Kolesnichenko, L.G., Vorobyev, S.N., Kirpotin, S.N., 2016a. Trace element transport in western Siberian rivers across a permafrost gradient. Biogeosciences 13, 1877–1900. https://doi.org/10.5194/bg-13-1877-2016.
Pokrovsky, O.S., Manasypov, R.M., Loiko, S.V., Shirokova, L.S., 2016b. Organic and organo-mineral colloids in discontinuous permafrost zone. Geochim. Cosmochim. Acta 188, 1–20. https://doi.org/10.1016/j.gca.2016.05.035.
Post, E., Alley, R.B., Christensen, T.R., Macias-Fauria, M., Forbes, B.C., Gooseff, M.N., Iler, A., Kerby, J.T., Laidre, K.L., Mann, M.E., Olofsson, J., Stroeve, J.C., Ulmer, F., Virginia, R.A., Wang, M., 2019. The polar regions in a 2°C warmer world. Sci. Adv. 5, eaaw9883. https://doi.org/10.1126/sciadv.aaw9883.
Poulin, B.A., Ryan, J.N., Tate, M.T., Krabbenhoft, D.P., Hines, M.E., Barkay, T., Schaefer, J., Aiken, G.R., 2019. Geochemical factors controlling dissolved elemental mercury and methylmercury formation in Alaskan wetlands of varying trophic status. Environ. Sci. Technol. 53, 6203–6213. https://doi.org/10.1021/acs.est.8b06041.
Praetorius, S.K., Condron, A., Mix, A.C., Walczak, M.H., McKay, J.L., Du, J., 2020. The role of Northeast Pacific meltwater events in deglacial climate change. Sci. Adv. 6, eaay2915. https://doi.org/10.1126/sciadv.aay2915.
Reimer, P.J., Austin, W.E.N., Bard, E., Bayliss, A., Blackwell, P.G., Bronk Ramsey, C., Butzin, M., Cheng, H., Edwards, R.L., Friedrich, M., Grootes, P.M., Guilderson, T.P.,

Hajdas, I., Heaton, T.J., Hogg, A.G., Hughen, K.A., Kromer, B., Manning, S.W., Muscheler, R., Palmer, J.G., Pearson, C., van der Plicht, J., Reimer, R.W., Richards, D.A., Scott, E.M., Southon, J.R., Turney, C.S.M., Wacker, L., Adolphi, F., Büntgen, U., Capano, M., Fahrni, S.M., Fogtmann-Schulz, A., Friedrich, R., Köhler, P., Kudsk, S., Miyake, F., Olsen, J., Reinig, F., Sakamoto, M., Sookdeo, A., Talamo, S., 2020. The IntCal20 northern hemisphere radiocarbon age calibration curve (0–55 cal kBP). Radiocarbon 62, 725–757. https://doi.org/10.1017/RDC.2020.41.

Rydberg, J., Klaminder, J., Rosén, P., Bindler, R., 2010. Climate driven release of carbon and mercury from permafrost mires increases mercury loading to sub-arctic lakes. Sci. Total Environ. 408, 4778–4783. https://doi.org/10.1016/j.scitotenv.2010.06.056.

Schaefer, K., Elshorbany, Y., Jafarov, E., Schuster, P.F., Striegl, R.G., Wickland, K.P., Sunderland, E.M., 2020. Potential impacts of mercury released from thawing permafrost. Nat. Commun. 11, 4650. https://doi.org/10.1038/s41467-020-18398-5.

Schneider, L., Cooke, C.A., Stansell, N.D., Haberle, S.G., 2020. Effects of climate variability on mercury deposition during the Older Dryas and Younger Dryas in the Venezuelan Andes. J. Paleolimnol. https://doi.org/10.1007/s10933-020-00111-7.

Schuster, P.F., Striegl, R.G., Aiken, G.R., Krabbenhoft, D.P., Dewild, J.F., Butler, K., Kamark, B., Dornblaser, M., 2011. Mercury export from the Yukon River basin and potential response to a changing climate. Environ. Sci. Technol. 45, 9262–9267. https://doi.org/10.1021/es202068b.

Schuster, P.F., Schaefer, K.M., Aiken, G.R., Antweiler, R.C., Dewild, J.F., Gryziec, J.D., Gusmeroli, A., Hugelius, G., Jafarov, E., Krabbenhoft, D.P., Liu, L., Herman-Mercer, N., Mu, C., Roth, D.A., Schaefer, T., Striegl, R.G., Wickland, K.P., Zhang, T., 2018. Permafrost stores a globally significant amount of mercury. Geophys. Res. Lett. 45, 1463–1471. https://doi.org/10.1002/2017GL075571.

Segato, D., Saiz-Lopez, A., Mahajan, A.S., Wang, F., Corella, J.P., Cuevas, C.A., Erhardt, T., Jensen, C.M., Zeppenfeld, C., Kjær, H.A., Turetta, C., Cairns, W.R.L., Barbante, C., Spolaor, A., 2023. Arctic mercury flux increased through the Last Glacial Termination with a warming climate. Nat. Geosci. 16, 439–445. https://doi.org/10.1038/s41561-023-01172-9.

Shelef, E., Griffore, M., Mark, S., Coleman, T., Wondolowski, N., Lasher, G.E., Abbott, M., 2022. Sensitivity of erosion-rate in permafrost landscapes to changing climatic and environmental conditions based on Lake sediments from northwestern Alaska. Earth's Future 10. https://doi.org/10.1029/2022EF002779.

Smith, M.I., Ke, Y., Geyman, E.C., Reahl, J.N., Douglas, M.M., Seelen, E.A., Magyar, J.S., Dunne, K.B.J., Mutter, E., Fischer, W.W., Lamb, M.P., West, A.J., 2024. Mercury stocks in discontinuous permafrost and their mobilization by river migration in the Yukon River Basin. Environ. Res. Lett. https://doi.org/10.1088/1748-9326/ad536e.

St. Pierre, K.A., Zolkos, S., Shakil, S., Tank, S.E., St. Louis, V.L., Kokelj, S.V., 2018. Unprecedented increases in total and methyl mercury concentrations downstream of retrogressive thaw slumps in the Western Canadian Arctic. Environ. Sci. Technol. 52, 14099–14109. https://doi.org/10.1021/acs.est.8b05348.

St. Pierre, K.A., St. Louis, V.L., Lehnherr, I., Gardner, A.S., Serbu, J.A., Mortimer, C.A., Muir, D.C.G., Wiklund, J.A., Lemire, D., Szostek, L., Talbot, C., 2019. Drivers of mercury cycling in the rapidly changing glacierized watershed of the high Arctic's largest lake by volume (Lake Hazen, Nunavut, Canada). Environ. Sci. Technol. 53, 1175–1185. https://doi.org/10.1021/acs.est.8b05926.

Staniszewska, K.J., Reyes, A.V., Cooke, C.A., Miller, B.S., Woywitka, R.J., 2022. Permafrost, geomorphic, and hydroclimatic controls on mercury, methylmercury, and lead concentrations and exports in Old Crow River, arctic western Canada. Chem. Geol. 596, 120810. https://doi.org/10.1016/j.chemgeo.2022.120810.

Streets, D.G., Horowitz, H.M., Jacob, D.J., Lu, Z., Levin, L., ter Schure, A.F.H., Sunderland, E.M., 2017. Total mercury released to the environment by human activities. Environ. Sci. Technol. 51, 5969–5977. https://doi.org/10.1021/acs.est.7b00451.

Tashiro, Y., Yoh, M., Shiraiwa, T., Onishi, T., Shesterkin, V., Kim, V., 2020. Seasonal variations of dissolved Iron concentration in active layer and rivers in permafrost areas. Russ. Far. East. Water 12, 2579. https://doi.org/10.3390/w12092579.

Thompson, L.M., Low, M., Shewan, R., Schulze, C., Simba, M., Sonnentag, O., Tank, S.E., Olefeldt, D., 2023. Concentrations and yields of mercury, methylmercury, and dissolved organic carbon from contrasting catchments in the discontinuous permafrost region, Western Canada. Water Resour. Res. 59, e2023WR034848. https://doi.org/10.1029/2023WR034848.

Wendler, G., Gordon, T., Stuefer, M., 2017. On the precipitation and precipitation change in Alaska. Atmosphere 8, 253. https://doi.org/10.3390/atmos8120253.

Wilson, C.R., Michelutti, N., Cooke, C.A., Briner, J.P., Wolfe, A.P., Smol, J.P., 2012. Arctic lake ontogeny across multiple interglaciations. Quat. Sci. Rev. 31, 112–126. https://doi.org/10.1016/j.quascirev.2011.10.018.

Zhang, T., Li, D., East, A.E., Walling, D.E., Lane, S., Overeem, I., Beylich, A.A., Koppes, M., Lu, X., 2022. Warming-driven erosion and sediment transport in cold regions. Nat. Rev. Earth Environ. 3, 832–851. https://doi.org/10.1038/s43017-022-00362-0.

Zhou, J., Obrist, D., Dastoor, A., Jiskra, M., Ryjkov, A., 2021. Vegetation uptake of mercury and impacts on global cycling. Nat. Rev. Earth Environ. 2, 269–284. https://doi.org/10.1038/s43017-021-00146-y.